Collision-induced dissociation of protonated uracil water clusters probed by molecular dynamics simulations

Sébastien Zamith, Linjie Zheng, Jérôme Cuny, Jean-Marc L'Hermite, Mathias Rapacioli

PCCP

ARTICLE TYPE

Cite this: DOI: 00.0000/xxxxxxxxxx

Collision-induced dissociation of protonated uracil water clusters probed by molecular dynamics simulations†

Linjie Zheng,[a] Jérôme Cuny,*[a] Sébastien Zamith,[b] Jean-Marc L'Hermite,[b] and Mathias Rapacioli*[a]

Received Date
Accepted Date

DOI: 00.0000/xxxxxxxxxx

Collision-induced dissociation experiments of hydrated molecular species can provide a wealth of important information. However, they often need a theoretical support to extract chemical information. In the present article, in order to provide a detailed description of recent experimental measurements [Braud *et al., J. Chem. Phys.* 2019, 150, 014303], collision simulations between low-energy protonated uracil water clusters $(H_2O)_{1-7,11,12}UH^+$ and an Ar atom were performed using a quantum mechanics / molecular mechanics formalism based on the self-consistent-charge density-functional based tight-binding method. The theoretical proportion of formed neutral *vs.* protonated uracil containing clusters, total fragmentation cross sections as well as the mass spectra of charged fragments are consistent with the experimental data which highlights the accuracy of the present simulations. They allow to probe which fragments are formed on the short time scale and rationalize the location of the excess proton on these fragments. We demonstrate that this latter property is highly influenced by the nature of the aggregate undergoing the collision. Analyses of the time evolution of the fragments populations and of their relative abundances demonstrate that, up to 7 water molecules, a direct dissociation mechanism occurs after collision whereas for 11 and 12 water molecules a statistical mechanism is more likely to participate. Although scarce in the literature, the present simulations appear as a useful tool to complement collision-induced dissociation experiments of hydrated molecular species.

1 Introduction

Collision-induced dissociation (CID) is a key tool to probe the structure, energetics and reactivity of a variety of molecular systems.[1,2] By colliding a molecule, or a molecular aggregate, with a non-reactive rare gas atom (Ne, Ar) or a small molecule such as H_2O or N_2, it is possible to monitor the parent ions and collision products by use, for instance, of tandem mass spectrometry (MS/MS).[3,4] The resulting mass spectra provide a wealth of information about the structure of the parent and product ions from which one can infer, for instance, dissociation mechanisms,[5,6] or bond and hydration enthalpies.[7] Similar information can also be obtained through other experiments such as threshold collision-induced dissociation,[8–10] black-body infrared radiative dissociation,[11–13] laser light dissociation,[14] or electron capture dissociation.[15,16] CID has been applied to a variety of systems, in particular hydrated atomic ions,[2,8,9,17,18] and molecular ions.[19–22] In the second case, it has been used to understand the impact of high-energy radiations on living cells and DNA or RNA,[23–25] as well as low-energy collisions on molecules of biological interest.[26,27]

Extracting energetics or dissociation mechanisms from CID is not an easy task and it often requires the use of complementary theoretical calculations. Two main methodologies can be conducted. The first one necessitates an exhaustive description of the potential energy surface (PES) connecting both parent ions and products. Energetic information on both minima and transition states can then be introduced in Rice-Ramsperger-Kassel-Marcus (RRKM)[28,29] and/or Kinetic Monte Carlo (KMC) simulations.[30,31] This first method is relevant for very late dissociations, occurring at times much larger than typical molecular vibrational periods. The second approach consists in performing molecular dynamics (MD) simulations to explicitly model the collision be-

[a] *Laboratoire de Chimie et Physique Quantiques LCPQ/IRSAMC, Université de Toulouse (UPS) and CNRS, 118 Route de Narbonne, F-31062 Toulouse, France. Fax: +33 (0)5 61 55 60 65; Tel: +33 (0)5 61 55 68 36; E-mail: mathias.rapacioli@irsamc.ups-tlse.fr; jerome.cuny@irsamc.ups-tlse.fr*

[b] *Laboratoire Collisions Agrégats Réactivié LCAR/IRSAMC, Université de Toulouse (UPS) and CNRS, 118 Route de Narbonne, F-31062 Toulouse, France.*

† Electronic Electronic Supplementary Material (ESI) available: Data for validation of the D_{NH} parameter ; Tests of statistical convergence with respect to the number of initial random conditions and *b* values ; Time-dependent proportion of fragments for a larger number of species and comparison with experimental data performed with Ne instead of Ar ; Tests of energy conservation along collision simulations ; coordinates of all considered isomers are provided in ESI. See DOI: 10.1039/cXCP00000x/ . Selected datasets can be downloaded from DOI : 10.5281/zenodo.5579070 .

tween the parent ion and the colliding species, the energy redistribution between the vibrational and rotational modes of the parent ion and the subsequent reorganizations and fragmentations. This approach can hardly describe statistical processes as it would require extremely long simulations. In contrast, it is particularly suitable to describe direct, *i.e.* non-statistical, dissociation mechanisms and often observed in CID studies.[32–35] This latter case requires the propagation of a large amount of independent trajectories to statistically converge the collision process. This necessitates a correct description of the PES of the system and its reactivity while maintaining a limited computational cost. Despite these difficulties, this approach has been widely used, in particular to study unimolecular reactivity on a short time scale.[36–47]

In contrast, theoretical and experimental studies devoted to dissociation of microhydrated molecular aggregates are scarce,[23,26,48–51] although CID has been applied to water clusters containing an atomic ion,[2,8,18] and on charged water clusters.[17,50,52,53] This is a real lack as microhydrated molecules and biomolecules represent valuable model systems that allow to understand the influence of hydration degree or protonation states by direct comparison between experiment and theory in a tractable way without having to consider complex long-range solvent effects. In that respect, CID investigations could play an important role in understanding structure, stability, dynamics and reactivity of species in an aqueous medium for different hydration degrees or protonation states. This can be evidenced by the experimental study of Liu *et al.* on the dissociation of the singly-charged adenosine 5'-monophosphate (AMP^-) which shows two different dissociation channel depending on the solvation state of AMP^-.[23] However, to the best of our knowledge, no modelling was performed to complement these experiments except for a few static calculations.[2,8,18]

In the present article, we aim at demonstrating that MD simulations based on a quantum chemical treatment of the PES are able to model such complex dissociation mechanism to provide an atomic-scale description that can not be obtained experimentally. To do so, we focus here on one particular system: protonated uracil (U) water clusters $(H_2O)_{1-7,11,12}UH^+$ colliding with an argon atom. This choice is motivated by the recent CID experiments performed by Braud *et al.* consisting in $(H_2O)_{1-15}UH^+$ clusters colliding with an impacting atom or molecule M (M = H_2O, D_2O, Ne, and Ar) at a constant center of mass collision energy of 7.2 eV.[54] This low value leads only to intermolecular bond breaking, without any electronic excitation, rather than intramolecular bond breaking. The authors determined the branching ratios for different charged fragments which allow them to deduce the fragmentation cross section for all $(H_2O)_{1-15}UH^+$ species and the location of the excess proton after collision: on a uracil containing cluster or on a pure water cluster. This leads to the proportion of neutral uracil loss (corresponding to cases where the excess proton is located on pure water clusters) as a function of the number n of water molecules. A sharp increase of neutral uracil loss was observed for n = 5-6 (2.8 and 25.0% for n = 4 and 7, respectively). Those experiment were complemented by theoretical calculations that aim at characterizing the lowest-energy isomers of $(H_2O)_{1-7}UH^+$ clusters. They show that (i) For n = 1-2, the uracil is protonated; (ii) For n = 3-4, the excess proton is still on the uracil but is closer to an adjacent water molecule than in case (i); (iii) When n is larger than 4, the excess proton is located on a water molecule. These results suggest that the location of the proton after collision recorded in the CID experiment is determined by its position in the lowest-energy parent isomer suggesting that a direct dissociation mechanism occurs. Despite these findings, static calculations can not provide a full picture for the dissociation process and some issues are still not properly understood: (i) What is the main path of the dissociation mechanisms ? (ii) What are the fragments after collision ? (iii) How does the proportion of fragments change according to time ? (iv) Is the proportion of neutral uracil loss only determined by the nature of the lowest-energy isomers ?

To answer these questions, the present article presents a complete MD study of the dissociation process for $(H_2O)_{1-7,11,12}UH^+$ aggregates colliding with an argon atom. The PES was described using a quantum mechanics / molecular mechanics formalism based on the self-consistent-charge density-functional based tight-binding (SCC-DFTB) method that allows for a quantum mechanical description of the systems while displaying a limited computational cost. The outline of the article is as follows: details on the SCC-DFTB and SCC-DFTB/MM approaches, exploration of potential energy surfaces, collisional trajectories and analysis is provided in the section 2. Section 3 discusses the theoretical time-dependent proportion of fragments, proportion of neutral uracil loss, total fragmentation cross sections and mass spectra of fragments bearing the excess proton. These data are compared to available experimental results in order to discuss in details dissociation mechanism as a function of n. The main outcomes and perspectives are summarized in section 4.

2 Computational Methods

SCC-DFTB potential. DFTB is an approximated DFT scheme whose computational efficiency relies on the use of parameterized integrals.[55–58] In this study, we used the second-order formulation of DFTB, the self-consistent-charge DFTB, in combination with the mio-set for the Slater-Koster tables of integrals.[56] To improve description of intermolecular interactions, the class IV/charge model 3 (CM3) charges were used instead of the original Mulliken charges as well as empirical terms to describe dispersion interactions.[59] For the parameterization of CM3 charges, the bond parameter D_{OH} = 0.129 proposed by Simon and coworkers was applied,[60,61] and a D_{NH} value of 0.120 was used (see Table S1 and Figure S1 in Electronic Supplementary Material (ESI)),[62] while all other bond parameters were set to 0.000, which corresponds to Mulliken evaluation of the charges. Over the last years, the accuracy of this model to describe water clusters has been demonstrated,[60–65] in particular, it has been applied to simulate collisions in various chemical systems.[64,66,67] Introduction of the CM3 charges also greatly improves the energetics of proton transfer events.[68] Interaction between argon and protonated uracil water cluster was treated with a SCC-DFTB/MM model,[69] which details can be found in the original paper.[70] This potential consists in a modification of the SCC-DFTB Hamiltonian matrix based on first order degenerate perturbation theory com-

bined with a polarization contribution. In practice, two scalar terms describe the interaction of Ar with the core electrons of the uracil water cluster and the dispersion potential between these two subsystems. A third non-scalar term describes the interaction between Ar and the valence electrons of the uracil water cluster. Finally, a polarisation term is added to account for the polarisation of the Ar atom by the uracil water cluster in a self consistent scheme. For the collision trajectories described below, a Fermi distribution (Fermi temperature 2000 K) was applied to avoid oscillation issues during the self-consistent procedure.[71] All the SCC-DFTB and SCC-DFTB/MM calculations were carried out with the deMonNano code.[72]

Determination of low-energy minima. All energy minima for $(H_2O)_{1-7}UH^+$ aggregates were obtained in a previous study following a two-step procedure.[54] The same procedure was conducted to obtain the low-energy isomers of $(H_2O)_{11}UH^+$ and $(H_2O)_{12}UH^+$. First, the PES of these two species was roughly explored using the parallel-tempering molecular dynamics (PTMD) algorithm in combination with SCC-DFTB.[73,74] 40 replicas with temperatures ranging linearly from 50 to 350 K were used. All trajectories were 4 ns long and the integration time step was 0.5 fs. A Nosé-Hoover chain of five thermostats with frequencies of 800 cm^{-1} was used to obtain an exploration in the canonical ensemble.[75,76] To avoid any spurious influence of the initial geometry on the PES exploration, three distinct PTMD simulations were carried out with distinct initial proton location: on the uracil in two cases and on a water molecule in the other one. In the former cases, we used two isomers reported as u178 and u138 UH^+ by Pedersen *et al.*.[77] 600 geometries per temperature were linearly selected along each PTMD simulation for subsequent geometry optimization leading to 72000 structures optimized at SCC-DFTB level. These structures were sorted in ascending energy order and checked for redundancy. 20 and 29 isomers were selected from these 72000 optimized structures and were subsequently optimized at the MP2/Def2TZVP level,[78,79] which leads to the low-energy isomers of $(H_2O)_{11}UH^+$ and $(H_2O)_{12}UH^+$, respectively. All MP2 calculations were carried out with the Gaussian 09 package.[80]

Collision trajectories. The aforementioned SCC-DFTB/MM approach was used to describe the collision process of protonated uracil water clusters (SCC-DFTB) and an argon atom (MM). Initial configurations for the collisional trajectories were set using the following procedure. The target cluster was first randomly rotated around its center of mass to allow collision with all possible impacting points on the cluster. 600 structures were generated per isomer in which the center of mass of the aggregate was kept at position (0, 0, 0). Convergence of the results with respect to the number of impacting orientation was tested and is discussed in the ESI (see Tables S2 and S3 as well as Figures S2 to S7). The colliding argon initial position was set at position (10, b, 0) where b is defined as the impact parameter. b was varied by step of 0.5 Å from 0 to R_{max}. Definition of R_{max}, number of considered b values for each isomer as well as convergence of the present results with respect to this number is presented in Table S4 in the ESI. This leads to $600\times(2R_{max}+1)$ initial configurations per isomer. For each one of them, initial velocities were defined such as the instantaneous temperature of the system was 25 K and its total momentum and total angular momentum were zero. 200 fs of simulation were subsequently performed in the canonical ensemble at 25 K using a stochastic velocity rescaling thermostat with a coupling parameter of 0.1 ps.[81] The influence of the duration of the equilibration process was tested and is presented in Table S5 of the ESI. These tests demonstrate that 200 fs of equilibration time is enough to capture the main properties of the dissociation mechanism. Then, the thermostat was turned-off and the impacting argon atom was given a velocity along the x axis corresponding to a center of mass collision energy E_{col} of 7.2 eV as used in the experiment.[54] 15 ps of simulation in the micro-canonical ensemble were accumulated. A time step of 0.5 fs was used for all collision trajectories which properly ensures energy conservation as demonstrated in the ESI.

Trajectory analysis. For data analysis, a fragment is defined as a group of atoms in which the distance of any pair of adjacent atoms is less than 5.0 Å. The number of hydrogen, nitrogen and oxygen atoms in one fragment is denoted by k, l and m, respectively. For instance, a fragment characterised by l=0 and k=2m+1 is a pure water cluster containing the excess proton. Identifying such a fragment at the end of the trajectory means that a neutral uracil fragment exists, otherwise the excess proton is located on a uracil containing fragment. In practice, at each time step, the fragments are identified on the basis of their k, l, m values, allowing to record their time-dependent evolution. The final mass spectrum is built by retaining only the fragments containing the excess proton, as only charged fragments are detected in the experiment. The proportion of neutral uracil loss (P_{NUL}) for simulations where dissociation occurred and the total fragmentation cross section (σ_{frag}) at a given center of mass collision energy E_{col} is derived from the following formula:

$$\begin{aligned} P_{NUL}(E_{col}) &= \int_0^{b_{max}} N_{NUL}(b,E_{col})2\pi b db \Big/ \int_0^{b_{max}} N_{frag}(b,E_{col})2\pi b db \\ &\simeq \frac{\sum_{i=0}^{b_{max}} \frac{1}{2}(N_{NUL}(b_i,E_{col})+N_{NUL}(b_{i+1},E_{col}))\pi(b_{i+1}^2-b_i^2)}{\sum_{i=0}^{b_{max}} \frac{1}{2}(N_{frag}(b_i,E_{col})+N_{frag}(b_{i+1},E_{col}))\pi(b_{i+1}^2-b_i^2)} \end{aligned} \quad (1)$$

$$\begin{aligned} \sigma_{frag}(E_{col}) &= \int_0^{b_{max}} P(b,E_{col})2\pi b db \quad (2) \\ &\simeq \sum_{i=0}^{b_{max}} \frac{1}{2}(P(b_i,E_{col})+P(b_{i+1},E_{col}))\pi(b_{i+1}^2-b_i^2) \end{aligned}$$

where $N_{NUL}(b,E_{col})$ and $N_{frag}(b,E_{col})$ are the total number of trajectories with a neutral uracil fragment at the end and the total number of trajectories leading to fragmentation as a function of the impact parameter b at E_{col}, respectively. $P(b,E_{col})$ is the opacity, *i.e.* the dissociation probability as a function of b at E_{col}. P_{NUL} and σ_{frag} are computed by averaging results over the $600\times(2R_{max}+1)$ simulations performed for each aggregate.

3 Results and Discussion

3.1 Time-dependent proportion of fragments

The time-dependent proportion of each fragment was extracted from collision trajectories. To illustrate the change in behavior resulting from the difference in cluster size, Figure 1 displays the time-dependent proportion of fragments obtained from the dissociation of the lowest-energy isomer of $(H_2O)_7UH^+$ (7a) and $(H_2O)_{12}UH^+$ (12a). For the sake of clarity, only the fragments displaying significant proportion, higher than 0.035 and 0.015 for 7a and 12a, respectively) are considered in these figures. This corresponds to the eight and ten most prominent fragments for 7a and 12a, respectively. Proportions of the main fragments of clusters 7d and 12c are displayed in Figure S8 in the ESI and display similar behavior as for 7a and 12a. From Figure 1, it is clear that for both aggregates, the proportion of H_2O has the sharpest increase after collision and then stay almost constant as a function of time. For 7a, ∼3 ps after collision, the proportion of almost all fragments does not change any more. Before that, the proportion of the $(H_2O)_6UH^+$ fragment increases first and then decreases, which indicates a sequential dissociation of water molecules. For 12a, proportion of $(H_2O)_{11}UH^+$ and $(H_2O)_{10}UH^+$ fragments displays a sharp increase quickly after collision which is then followed by a fast decrease, and finally it keeps a minute decrease up to the end of the simulations. The decrease of proportion of $(H_2O)_{10}UH^+$ and $(H_2O)_{11}UH^+$, and the increase of proportion of $(H_2O)_6UH^+$, $(H_2O)_7UH^+$ and $(H_2O)_8UH^+$ indicate that sequential dissociation after collision is occurring. It is worth noting that, in contrast to 7a, the proportions of the main fragments of 12a do not tend to be a constant at the end of the simulations. This implies that, for this large aggregate, structural rearrangements are more likely to occur prior to complete dissociation. As a first conclusion, Figure 1 suggests that clusters with 7 water molecules experience a direct dissociation mechanism as was hypothesised by Braud *et al.*.[54] A similar conclusion can be drawn for smaller cluster sizes as supported by Figure S9-S11 in the ESI, although a few exceptions can be observed, in particular a non negligible time evolution of $(H_2O)_2UH^+$ proportion above 10 ps of simulation for the collision of isomer 4a. In contrast, cluster with 12 water molecules shows a behaviour compatible with a certain amount of statistical dissociation, namely a long-time evolution that allows structural rearrangements. A similar conclusion can be drawn for $(H_2O)_{11}UH^+$ as supported by Figure S12 in the ESI. These important observations can now be refined by looking at more detailed properties.

3.2 Proportion of neutral uracil loss and total fragmentation cross sections for small clusters

In order to get more insight in the fragmentation, molecular dynamics trajectories were analysed in terms of proportion of neutral uracil loss (P_{NUL}) and total fragmentation cross sections (σ_{frag}) as defined in section 2 in equations 1 and 2, respectively. These two properties are also accessible from experiments. Another property extracted from the MD simulations, but not accessible from experiment, is the proportion of protonated uracil (P_{PU}) which is equal to the ratio of the number of simulations leading to an aggregate containing a protonated uracil molecule over the number of simulations leading to a fragment containing the uracil and the excess proton, not necessary bound together. In order to correlate the outcome of the collision and the structure of the aggregate undergoing the collision, all considered low-energy isomers are characterized by there relative energies ($E_{rel.}$) and the location of the excess proton (LEP). For the latter, three distinct configurations were considered: The excess proton is bounded to the uracil molecule (noted U-H); The excess proton is bounded to a water molecule that is adjacent to an oxygen atom of the uracil molecule (noted W-H-U); The excess proton is bounded to a water molecule that is separated by at least one other water molecule from the uracil molecule (noted W-H). All these data are gathered in Table 1 and we first discuss the behaviour of the small species $(H_2O)_{1-7}UH^+$.

Various information can be inferred from these properties. Firstly, one observes a general increase of σ_{frag} as a function of cluster size with values ranging from 25.9 Å^2 for isomer 1b to 60.2 Å^2 for isomer 12a. Interestingly, only slight variations of σ_{frag} are observed for different isomers of the same aggregate. In contrast, P_{NUL} is much more sensitive to the nature of the considered isomers, in particular when these isomers display different LEP values. For instance, P_{NUL} is 46.6 % for 5a (W-H) while it is only 0.1 % for 5d (U-H). More interestingly, there seems to exist a strong correlation between P_{NUL} and LEP. Indeed, P_{NUL} values below 1.0 % are characterized by an excess proton initially bounded to uracil (U-H type). This suggests that when uracil is protonated, probability for deprotonation after collision is very low and thus P_{NUL} is close to 0%. P_{NUL} values between 9.7 and 29.4 % are obtained from W-H-U configurations while larger P_{NUL} values, above 31.1 %, arise from W-H configurations in clusters $(H_2O)_{5-7}UH^+$. This demonstrates that, from the excess proton point of view, the outcome of the collision is highly sensitive to the nature of the isomer undergoing the collision as hypothesised by Braud et al.[54] This important finding can be of help to determine which isomer, or set of isomers, is likely to undergo collision by comparing experimental and theoretical P_{NUL} as this is not necessarily the lowest-energy isomer as discussed below.

For $(H_2O)_{1-2}UH^+$, the theoretical and experimental P_{NUL} values, close to zero, are in good agreement regardless of the considered isomer. For $(H_2O)_3UH^+$, the experimental P_{NUL} is 1.7 % which is well reproduced by both isomers 3a and 3b although 3b is the one closer to the experimental value, 0.0 % against 5.7 % for 3a. This was expected as they are very close in energy, only 0.3 kcal.mol^{-1} difference, and in structure, as displayed in Figure 2, both being of U-H type structure. Consequently, in the experiment, each one of them could be at the origin of the experimental signal. $(H_2O)_4UH^+$ behaves differently. The two low-energy isomers, 4a and 4b, display very different P_{NUL} values, 29.4 and 2.6 %, respectively. The experimental value is 2.8 % which suggests that 4b, although slightly higher in energy by 0.9 kcal.mol^{-1}, is the isomer prevailing during the collision process. The difference in behaviour can be explained by the U-H configuration of 4b, in which the excess proton is bounded to the uracil, whereas in 4a, it is bounded to a water molecule adjacent to uracil (see Figure 3). The case of $(H_2O)_5UH^+$ is more complex

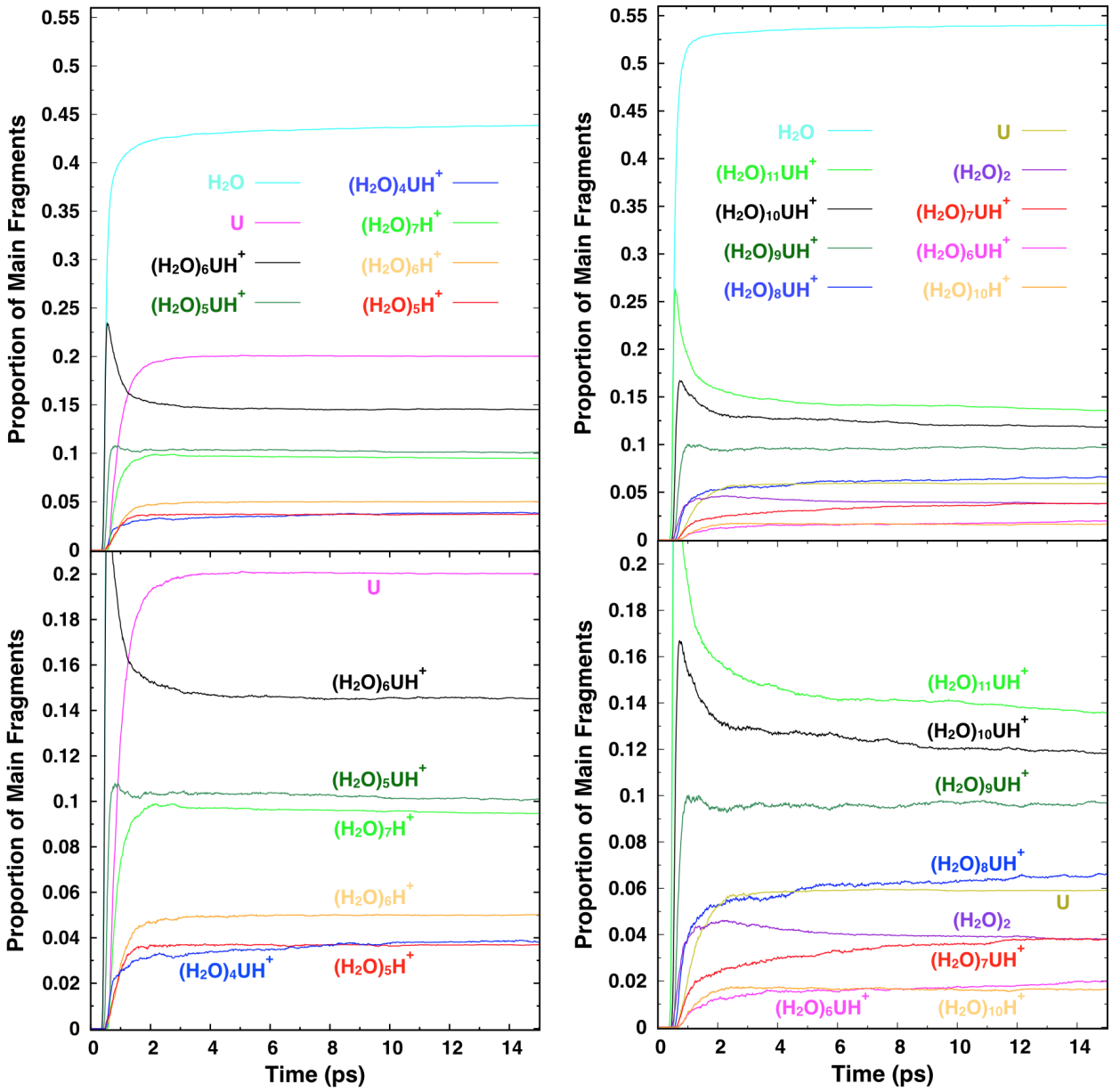

Fig. 1 Theoretical time-dependent proportions of the main fragments obtained from the dissociation of the lowest-energy isomers of $(H_2O)_7UH^+$ (left) and $(H_2O)_{12}UH^+$ (right). Bottom panels correspond to a zoom over the lower proportions.

as this is the first species displaying the three types of LEP configuration among its four lowest-energy isomers as can be seen on Figure 3. This implies very different P_{NUL} values: 46.6 % for 5a, 28.5 and 27.1 % for 5b and 5c, respectively, while it is only 0.1 % for 5d. The experimental P_{NUL} value for $(H_2O)_5UH^+$ is still relatively low, 7.5 %, which suggests that a U-H type structure prevails during the collision process. Although 5d is 2.4 kcal.mol^{-1} higher in energy than 5a, this isomer is thus expected to undergo the collision.

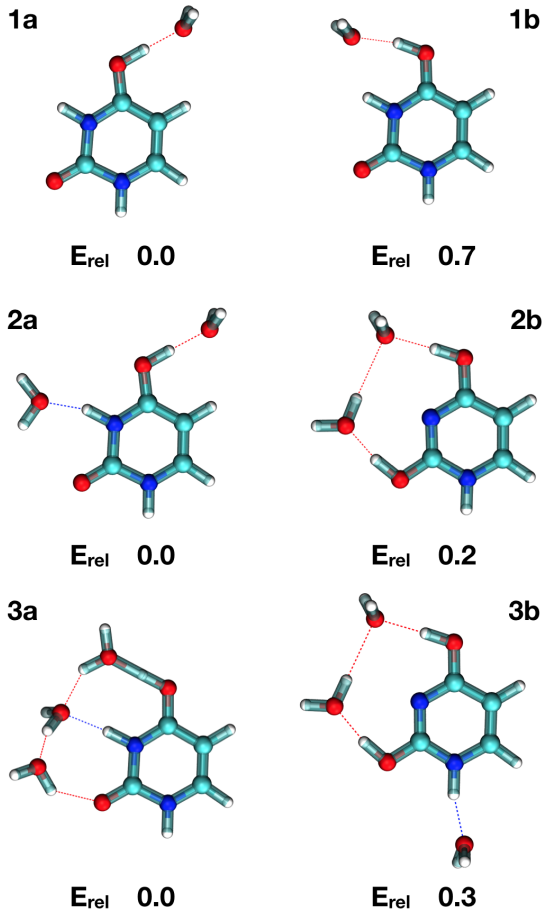

Fig. 2 Selected low-energy configurations of $(H_2O)_{1-3}UH^+$. Relative energies at the MP2/Def2TZVP level are in kcal.mol^{-1}.

$(H_2O)_6UH^+$ and $(H_2O)_7UH^+$ are the first two aggregates for which no low-energy isomer belongs to the U-H type structure. As a consequence, in contrast to smaller species, the theoretical P_{NUL} values are all higher than 15 %. This is in line with the experimental values which display a net increase at $n = 6$. Isomers 6a, 6b, 6c, 6d, and 6e (see Figure 4) are all W-H type structures which leads to P_{NUL} values almost twice higher than the experimental one. Consequently, as for $(H_2O)_5UH^+$, one can assume that the isomer of $(H_2O)_6UH^+$ undergoing the collision is more likely to be a W-H-U type structure although it is higher in relative energy. Isomer 6f can be such a candidate as it displays of P_{NUL} value of 18.5% which is in agreement with the experimental value, 18.0%. Due to its increasing size, $(H_2O)_6UH^+$ displays W-H configurations with the excess proton at various distances from

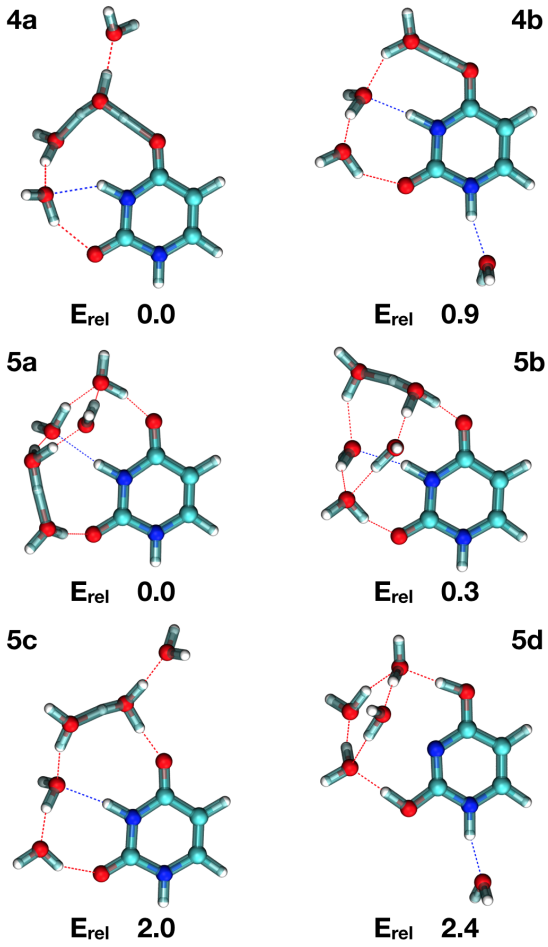

Fig. 3 Selected low-energy configurations of $(H_2O)_{4-5}UH^+$. Relative energies at the MP2/Def2TZVP level are in kcal.mol^{-1}.

the recombining oxygen. Indeed, in 6a, 6c and 6d this distance is 1.774, 1.745 and 1.804 Å, while in 6b, 6e and 6f, it is shorter: 1.660, 1.614, and 1.494 Å, respectively. However, no net correlation is observed between this distance and the value of P_{NUL}: 39.3, 33.8, 36.6, 34.7, 34.9 and 18.5% for 6a, 6b, 6c, 6d, 6e and 6f, respectively. In particular, the behaviour of 6e is striking. It has almost the same relative energy as 6f and they are structurally similar (see Figure 4) but display different P_{NUL} values. This suggests that, for n larger than 5, the ability of the water molecule network to stabilise the excess proton, *i.e* to promote or prevent its diffusion toward the uracil molecule, starts to be competitive with the configuration type of the isomer. In 6e, the excess proton is in a configuration close to the Zundel ion which may explain its high P_{NUL} value as compared to 6f. For $(H_2O)_7UH^+$, a W-U-H type configuration is also expected to fit best to the experimental result. And indeed 7d, a W-H-U type structure, which is only 0.8 kcal.mol^{-1} above the lowest-energy isomer (see Figure 5), has a P_{NUL} value of 22.9 % as compared to 25.0 % experimentally. Isomers 7a and 7c have a W-H configuration and their P_{NUL} values (31.3 and 31.1 %, respectively) are higher than the ones of 7b and 7d which have a W-H-U configuration.

Finally, it is worth noting that even when the excess proton is initially bounded to a water molecule, *i.e.* when a W-H type struc-

Table 1 Relative energy $E_{rel.}$ (in kcal.mol^{-1}) at the MP2/Def2TZVP level, LEP, P_{PU} (in %), P_{NUL} (in %), σ_{frag} (in Å^2) of the considered low-energy isomers of $(H_2O)_{1-7,11,12}UH^+$ clusters. Isomers which P_{NUL} fit best to the experimental value are indicated in bold. $P_{NUL_{exp}}$ and $\sigma_{frag_{exp}}$ are the experimental values for P_{NUL} and σ_{frag}, respectively. The standard error calculated for $P_{NUL_{exp}}$, evaluated over 5 independent measurements of each experimental value, is provided in parenthesis for $(H_2O)_{1-7,11}UH^+$. For $(H_2O)_{12}UH^+$, only one measurement was performed, so no standard error can be provided. For $(H_2O)_{12}UH^+$, experimental values were obtained for collision with Ne, whereas all other theoretical and experimental data are for collision with Ar.

Isomers	$E_{rel.}$	LEP	P_{PU}	P_{NUL}	$P_{NUL_{exp}}$	σ_{frag}	$\sigma_{frag_{exp}}$
1a	0.0	U-H	100	0.2	0.9 (0.6)	28.9	12.3
1b	0.7	U-H	100	0.1		25.9	
2a	0.0	U-H	100	0.0	0.4 (0.9)	36.3	22.8
2b	0.2	U-H	100	0.1		34.9	
3a	0.0	U-H	100	5.7	1.7 (1.9)	36.3	31.2
3b	0.3	U-H	100	0.0		41.9	
4a	0.0	W-H-U	98.0	29.4	2.8 (0.2)	40.1	43.4
4b	0.9	U-H	99.7	2.6		45.2	
5a	0.0	W-H	78.5	46.6	7.5 (0.4)	38.2	48.0
5b	0.3	W-H-U	89.0	28.5		38.7	
5c	2.0	W-H-U	87.8	27.1		44.6	
5d	2.4	U-H	100	0.1		47.5	
6a	0.0	W-H	44.1	39.3	18.0 (0.7)	45.8	54.3
6b	0.2	W-H	43.5	33.8		58.6	
6c	0.3	W-H	46.4	36.6		46.1	
6d	0.9	W-H	64.6	34.7		42.6	
6e	2.5	W-H	45.9	34.9		50.5	
6f	2.7	W-H-U	76.2	18.5		55.0	
7a	0.0	W-H	28.2	31.3	25.0 (0.8)	53.4	59.7
7b	0.3	W-H-U	52.4	21.4		51.7	
7c	0.3	W-H	41.3	31.1		49.5	
7d	0.8	W-H-U	40.9	23.0		54.0	
11a	0.0	W-H	4.6	28.3	11.8 (2.1)	52.9	63.8
11b	1.4	W-H	3.2	28.5		54.7	
11c	1.5	W-H	4.2	22.8		55.2	
11d	1.9	W-H	6.8	15.6		56.5	
11e	1.9	W-H	5.4	22.7		52.6	
11f	2.3	W-H	7.9	24.3		52.0	
12a	0.0	W-H	6.7	7.6	12.2	60.2	77.0
12b	0.6	W-H	34.0	22.4		52.2	
12c	0.7	W-H	48.7	10.8		55.4	
12d	1.3	W-H-U	5.4	9.7		54.3	
12e	1.8	W-H-U	67.5	6.0		54.2	
12f	2.4	W-H-U	55.0	17.1		54.1	

ture is considered, the maximum P_{NUL} that has been obtained is only 46.6 %. This demonstrates that for small aggregates such as $(H_2O)_{5-7}UH^+$ (smaller ones do not display low-energy W-H type structures), dissociation mainly lead to protonated uracil containing fragments. This is in line with the experimental results. Analysis of P_{PU} values also show that uracil is protonated in a significant amount of these protonated uracil containing fragments. P_{PU} has a clear tendency to decrease with cluster size, but can be quite high even for W-H type structures, see for instance 5a, 6d and 7c in Table 1. This demonstrates that upon collision, the excess proton is likely to transfer to uracil on a rather short time scale.

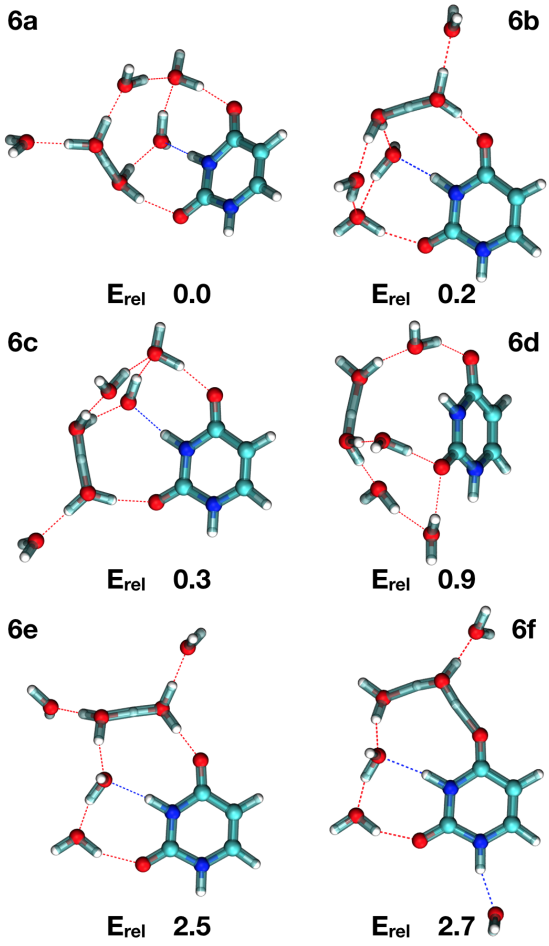

Fig. 4 Selected low-energy configurations of $(H_2O)_6UH^+$. Relative energies at the MP2/Def2TZVP level are in kcal.mol^{-1}.

The clusters discussed above exhibit a complex potential energy surfaces characterized by several low-energy isomers, with relative energies that can be lower than 1 kcal.mol^{-1}, and which get more complex as the number of water molecules increases. Consequently, the exact energetic ordering between the low-energy isomers can not be precisely known as this is below chemical accuracy and we thus can not claim to know for sure the lowest-energy structure of each aggregate. Furthermore, experimental, there is also no certainty that the isomer undergoing the collision is the lowest-energy isomer. Nevertheless, what we show is that P_{NUL} is mainly determined by the initial position of the proton in

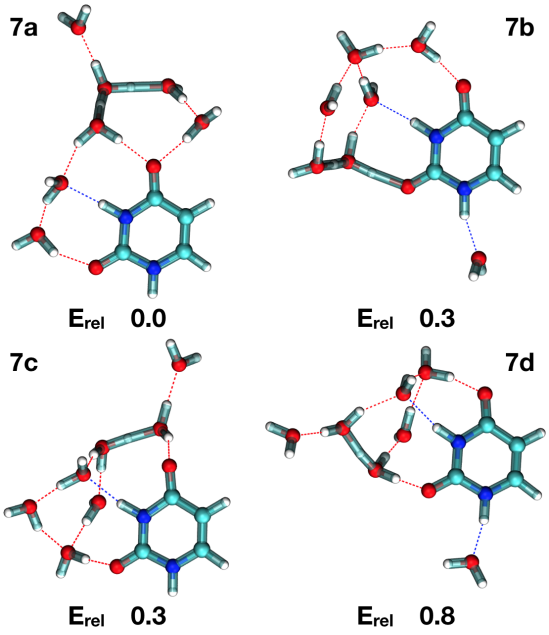

Fig. 5 Selected low-energy configurations of $(H_2O)_7UH^+$. Relative energies at the MP2/Def2TZVP level are in kcal.mol^{-1}.

the isomer undergoing the collision. Consequently, for the collision energy and the range of cluster size we have considered, the structure of the aggregate undergoing the collision is key in determining the dissociation process and collision outcomes much more than energetics. This is consistent with the analysis of the time-dependent proportion of fragments which suggests a direct dissociation mechanism. This is further highlighted on Figure 6, which presents the experimental P_{NUL} as a function of n and the corresponding theoretical values obtained from the lowest-energy isomers as well as from a set of isomers for which P_{NUL} matches the experimental data. This second set of isomers demonstrates that among the variety of low-energy isomers we were able to locate, there is always one of them which collision properties matches well the experimental data. This particular isomer can thus be proposed as the one undergoing the collision although it is not the lowest-energy one. Interestingly, if a similar plot is drawn for σ_{frag} considering the same isomers (see Figure 7), a good agreement with the experimental data is also obtained with the two sets of isomers which confirms the weaker dependence upon isomer of σ_{frag}. Comparison with the geometrical cross-section σ_{geo} also demonstrates that explicit molecular dynamics simulations as performed in the present study have a much better capability to capture the physics of the collision whereas a simple geometrical model considering spherical aggregates is too crude.

3.3 Behaviour at larger sizes, the case of $(H_2O)_{11}UH^+$ and $(H_2O)_{12}UH^+$

In the experiments conducted by Braud *et al.*,[54] P_{NUL} starts to decrease at n=8. This decrease is not consistent with the above argument of a direct dissociation mechanism and larger species more likely characterized by W-H and W-H-U type structures. This apparent discrepancy motivated us to extend the present study to

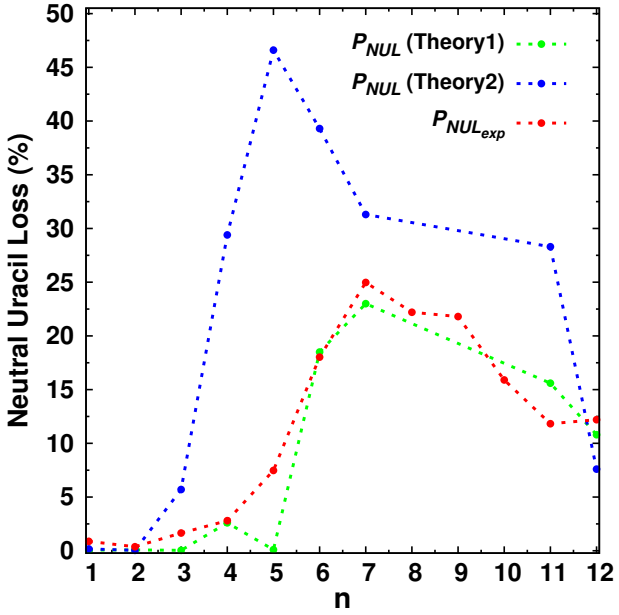

Fig. 6 Theoretical (green and blue lines) and experimental (red line) P_{NUL} values for the $(H_2O)_{1-7,11,12}UH^+$ clusters. Theory 1 (green line) is obtained from the isomers which P_{NUL} matches best to the experimental data (identified in Table 1 by bold characters) while Theory 2 (blue line) is obtained from lowest-energy isomers. For $(H_2O)_{12}UH^+$, experimental values were obtained for collision with Ne, whereas all other theoretical and experimental data are for collision with Ar.

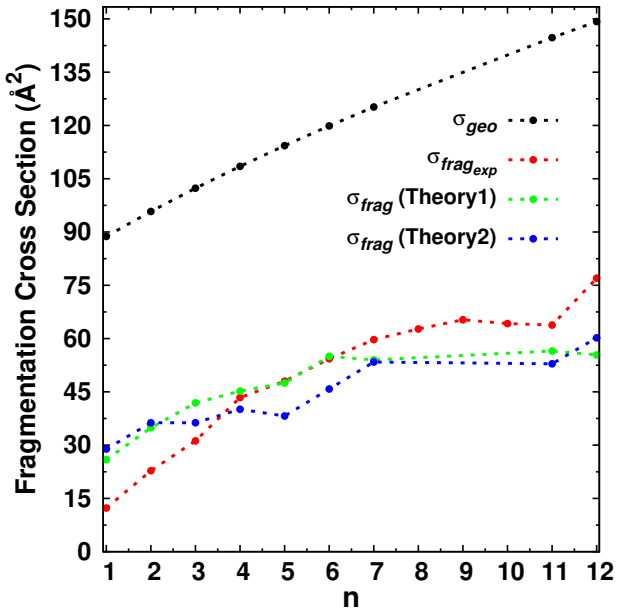

Fig. 7 Theoretical (green and blue lines) and experimental (red line) σ_{frag} values for the $(H_2O)_{1-7,11,12}UH^+$ clusters. Theory 1 (green line) is obtained from the isomers which P_{NUL} matches best to the experimental data (identified in Table 1 by bold characters) while Theory 2 (blue line) is obtained from lowest-energy isomers. For $(H_2O)_{12}UH^+$, experimental values were obtained for collision with Ne, whereas all other theoretical and experimental data are for collision with Ar.

larger clusters, namely $(H_2O)_{11}UH^+$ and $(H_2O)_{12}UH^+$. For the latter, the only available experimental data is for collisions with Ne instead of Ar, although for the same center of mass collision energy. As shown in Figures S13 and S14 of ESI, experimental P_{NUL} and σ_{frag} values for Ne or Ar, although not equal, display similar trend. In the following, we thus discuss the experimental data of $(H_2O)_{12}UH^+$ colliding with Ne.

The behaviour for $(H_2O)_{11}UH^+$ and $(H_2O)_{12}UH^+$ is rather different when looking at detailed properties. Indeed, for $(H_2O)_{11}UH^+$, P_{NUL} values for isomers 11a, 11b, 11c, 11e, and 11f are very similar as they range from 22.7 to 29.8 %. For 11d, P_{NUL} equal 15.6 % which fits best to the experiment. These P_{NUL} values are lower than those of $(H_2O)_6UH^+$, as observed experimentally, and in the same range as $(H_2O)_7UH^+$. All isomers display a W-H type configuration as seen in Figure 8. P_{PU} is very small for all $(H_2O)_{11}UH^+$ isomers which shows that on the time scale of the simulations, protonation of uracil hardly occurs. For $(H_2O)_{12}UH^+$, 12c isomer, which has a W-H type configuration (see Figure 9), has a P_{NUL} value which fits best to the experiment, 10.8 % against 12.2 %, while isomer 12a, also a W-H type configuration (see Figure 9), has a P_{NUL} value equal to 7.6 %. Overall, P_{NUL} values calculated for $(H_2O)_{12}UH^+$ isomers are lower than those of $(H_2O)_6UH^+$ and $(H_2O)_7UH^+$, which is in line with the experiment. The main difference with the $(H_2O)_{1-7}UH^+$ aggregates is that no clear relation exist between the P_{NUL} value and the initial localisation of the excess proton. Indeed, 12a, 12b and 12c are all W-H type configurations but with P_{NUL} values ranging from 7.6 to 22.4 %. The same is observed for 12d, 12e and 12f although they are all W-H-U type configurations. Similarly, no difference in behaviour is obtained between W-H and W-H-U type configurations. This can be explained by assuming that the dissociation mechanism in $(H_2O)_{12}UH^+$ involves some amount of structural rearrangement that softens the impact of the isomer undergoing the collision. Indeed, as $(H_2O)_{12}UH^+$ has more degrees of freedom, it can more easily accommodate the kinetic energy transferred by the colliding atom prior to dissociation which thus takes place on a longer time scale. This excess of internal energy thus fosters structural rearrangements, in particular proton transfers toward the uracil, explaining the smaller P_{NUL} value for $(H_2O)_{12}UH^+$. This is in full agreement with the conclusions obtained in section 3.1 from the data of Figure 1. To further support this conclusion, we conducted 200 MD simulations in the microcanonical ensemble in which the whole kinetic energy of Ar was randomly distributed in all the vibrational modes of isomer 12c by drawing initial velocities in a 1185 K Boltzmann distribution. Among them, 166 simulations display dissociation with one or two water molecules dissociating from the main cluster. No neutral uracil loss is observed. To conclude, although the present simulations are too short to assert that $(H_2O)_{12}UH^+$ undergoes a statistical dissociation mechanism, they clearly show that a direct mechanism is not sufficient to account for the theoretical and experimental results. Consequently, structural rearrangements are very likely to occur prior to dissociation and the experimental results for P_{NUL} and σ_{frag} values can not result from the direct dissociation of a single $(H_2O)_{12}UH^+$ isomer. In contrast, similarities in both P_{NUL} and P_{PU} values for all considered $(H_2O)_{11}UH^+$

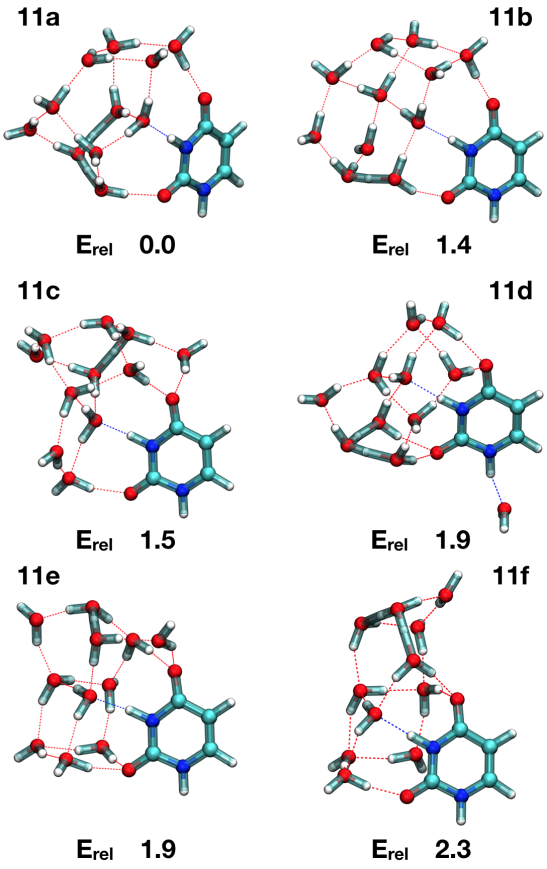

Fig. 8 Selected low-energy configurations of $(H_2O)_{11}UH^+$. Relative energies at the MP2/Def2TZVP level are in kcal.mol^{-1}.

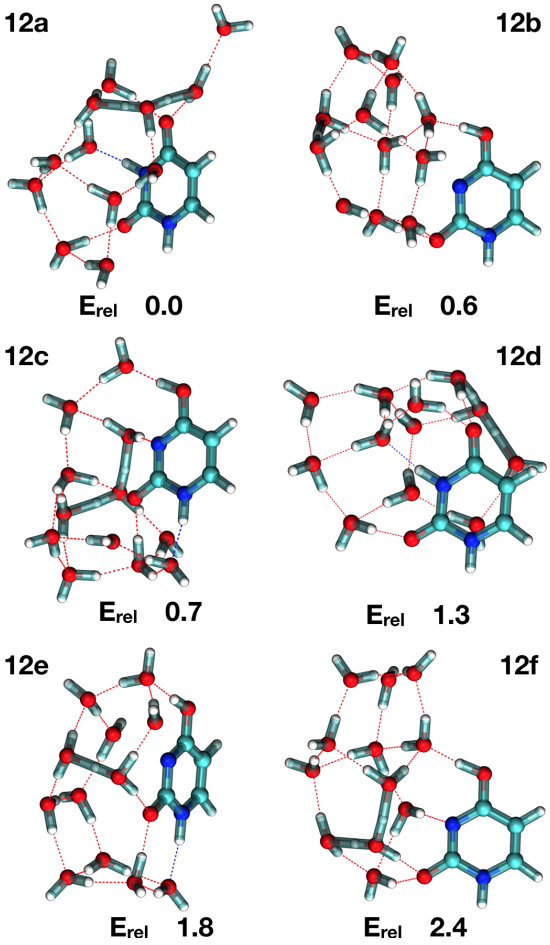

Fig. 9 Selected low-energy configurations of $(H_2O)_{12}UH^+$. Relative energies at the MP2/Def2TZVP level are in kcal.mol^{-1}.

isomers do not evidence structural rearrangements in this species although this does not mean they can not occur.

3.4 Mass spectrum of fragments with excess proton

In this last section, in order to analyse in more details collision products, the branching ratios of the different fragments containing the excess proton were extracted from the collision simulations of clusters $(H_2O)_{1-7,11,12}UH^+$ and compared with the experimental ones shaped as mass spectra.[54] For each cluster size, only simulations corresponding to the isomer which P_{NUL} value fits best to the experiment were considered (1a, 2b, 3b, 4b, 5d, 6f, 7d, 11d, 12c). The results are presented in Figure 10 and S15. For $(H_2O)_{12}UH^+$, there is no experimental data for collision with argon we thus discuss the experimental results obtained for collision with Ne. For comparison, all experimental data obtained from collision with Ne are also presented in Figure S16 in the ESI.

Overall, the experimental and theoretical spectra present the same general trends: (i) The mass spectra present a broad distribution of sizes, without prominence of a particular peak; (ii) All the spectra are dominated by the heaviest protonated uracil containing fragment (loss of a single water molecule) with the exception of the simulated mass spectrum for $(H_2O)_2UH^+$; (iii) Fragments containing protonated uracil prevail over pure protonated water fragments, as already observed from the P_{NUL} values provided in Table 1; (iv) Pure protonated water fragments only appear for the largest cluster sizes. Indeed, although very minor contributions are observed in both the simulated and experimental spectra for parent clusters with n=3-5, significant contributions of these species only appear when the parent cluster contains at least 6 water molecules.

We now turn to a more detailed discussion of the simulated and experimental mass spectra. For $(H_2O)_2UH^+$, fragments $(H_2O)UH^+$ and UH^+ are observed in both experiment and theory although their relative ratio is different. For $(H_2O)_3UH^+$, the simulated and experimental spectra agree quite well with a dominant peak for $(H_2O)_2UH^+$. For $(H_2O)_4UH^+$, in both experimental and theoretical spectra, the peak intensity of the fragments containing protonated uracil increases with the number of water molecules. For $(H_2O)_5UH^+$ and $(H_2O)_6UH^+$, this is also the case except for the UH^+ fragment which is overestimated when compared to the experimental result in Figure 10 (e). For $(H_2O)_7UH^+$, $(H_2O)_{11}UH^+$ and $(H_2O)_{12}UH^+$, the intensities for the heaviest fragments are overestimated, whichever their nature.

From Figure 10, it is clear that the smaller the cluster (except Figure 10 (b)) is, the better the agreement between the simulated and experimental branching ratios is. This trend indicates that for small clusters, *i.e.* for $n = 1-6$, short simulation time is enough to capture the full dissociation pattern, in other words, the dis-

Table 2 Energies of five $(H_2O)_6UH^+$ fragments selected from the dissociation of 7d at SCC-DFTB level, and the energies of the lowest-energy isomer of $(H_2O)_5UH^+$ and (H_2O) at SCC-DFTB level. The relative energy $\Delta E = E_{(H_2O)_6UH^+}$ -($E_{(H_2O)_5UH^+} + E_{H_2O}$). All energies are given in eV.

$E_{(H_2O)_6UH^+}$	$E_{(H_2O)_5UH^+}$	E_{H_2O}	ΔE
-44.310	-40.312	-4.057	1.605
-44.322	-40.312	-4.057	1.279
-44.307	-40.312	-4.057	1.687
-44.344	-40.312	-4.057	0.680
-44.373	-40.312	-4.057	-0.109

sociation mechanism is direct with no noticeable contribution of long term evolution. However, for larger clusters, starting at n=7, owing to the larger number of degrees of freedom, short simulation time does not capture the full dissociation pattern, *i.e.* long term statistical dissociation is more likely to play a noticeable role. This is fully in line with the conclusions obtained in section 3.3 for $(H_2O)_{12}UH^+$ and refine the interpretation given in section 3.2 for $(H_2O)_7UH^+$. This also shows that although the data presented in section 3.3 for $(H_2O)_{11}UH^+$ do no evidence the contribution of structural re-arrangements on the short time scale, they are very likely to occur as in $(H_2O)_{12}UH^+$.

One has to keep in mind that modelling the complete duration of the experiment (up to μs) is out of reach with MD/SCC-DFTB simulations. In the present study the simulation time was 15 ps, for all cluster sizes. Large fragments such as $(H_2O)_{6-12}UH^+$ may lose more water molecules if long enough simulation time were available, as suggested from the time-dependent evolution of selected trajectories in section 3.1. To certify this, we calculated at the SCC-DFTB level the total energy of the $(H_2O)_6UH^+$ fragments originating from the dissociation of $(H_2O)_7UH^+$ (7d). The calculation was performed on the 1421 trajectories producing the $(H_2O)_6UH^+$ fragment among the 9000 trajectories conducted for this particular isomer, *i.e.* 15.8 %. We then subtract the SCC-DFTB energies of the 5a isomer and H_2O. For visual illustration, the deduced relative energies ΔE are reported in Table 2 for five cases. When ΔE is greater than zero, it is possible for the $(H_2O)_6UH^+$ fragment to lose a water molecule. The percentage of ΔE being positive in all the trajectories leading to $(H_2O)_6UH^+$ fragment is 53.0 %, which indicates that many $(H_2O)_6UH^+$ fragments have still the potential to lose one more water molecule after the end of the simulation.

4 Conclusions

Collision-induced dissociation of protonated uracil water clusters $(H_2O)_{1-7,11,12}UH^+$ at constant center of mass collision energy has been investigated by molecular dynamics simulations using the SCC-DFTB method. The very good agreement between the simulated and measured P_{NUL} and σ_{frag} as well as branching ratios indicate that the essence of the dissociation induced by collisions is well captured by the simulations.

The P_{NUL} values from the different isomers of the $(H_2O)_{1-7}UH^+$ cluster show that the localization of the excess proton after dissociation is strongly determined by the initial configuration of the isomer undergoing the collision. This suggests that $(H_2O)_{1-7}UH^+$ aggregates primarily engage a direct dissociation path after collision that takes place on a very short time scale, *i.e.* lower than 15 ps. More strikingly, in most cases, the proposed lowest-energy isomer does not lead to the best fit to the experiment. However, the relative energy between the lowest-energy isomers and the isomers best fitting to the experiment is less than 1.0 kcal.mol^{-1} for $(H_2O)_{1-4,7}UH^+$ clusters and less than 2.7 kcal.mol^{-1} for $(H_2O)_{5,6}UH^+$ clusters. This is in line with the strong sensitivity of the collision outcome with the nature of the isomer undergoing the collision. This even suggests that the LEP can help in determining the main characteristic of the isomer involved in the collision. For $(H_2O)_{12}UH^+$, these conclusions do not apply any more which shows that significant structural rearrangements occur after collision. This is confirmed by the time-dependent proportion of fragments which continue to vary even at 15 ps for $(H_2O)_{12}UH^+$ whereas it is almost flat for $(H_2O)_7UH^+$. Analysis of the fragment branching ratios helps in clarifying these points. Indeed, for the smallest clusters, $(H_2O)_{1-5}UH^+$, the short simulation time well reproduces the corresponding experimental results which is in line with a direct mechanism. In contrast, for $(H_2O)_{6-7}UH^+$, although P_{NUL} is well reproduced by the simulations, the experimental and theoretical branching ratios differ which shows that more time is needed to properly describe the dissociation. For $(H_2O)_{11-12}UH^+$, theoretical and experimental branching ratios differ even more significantly which is a strong indication that a significant contribution of structural rearrangements occur. This suggests that a contribution of a statistical mechanism is more likely to occur for larger species such as $(H_2O)_{11-12}UH^+$.

The present study demonstrates that explicit molecular dynamics simulations performed at a quantum chemical level can provide a wealth of information about collision-induced mechanism in molecular clusters, in particular, hydrated molecular species. Such simulations thus represent a key tool to complement CID experiments and we hope the present study will motivate similar computational studies on future CID experiments of hydrated molecular aggregates. In a near future, we think it would be of great interest to pursue this study by looking at the influence of collision energy, both lower or higher, on the dissociation mechanism as a function of the cluster size. Furthermore, inclusion of nuclear quantum effects in the simulations could also help to increase the accuracy of the model and improve the comparison with the experiments.

Conflicts of interest

There are no conflicts to declare.

Acknowledgements

The authors acknowledge the supercomputing facility of CALMIP for generous allocation of computer resources (projects P1320 and P0059). The authors declare that there has been no significant financial support for this work.

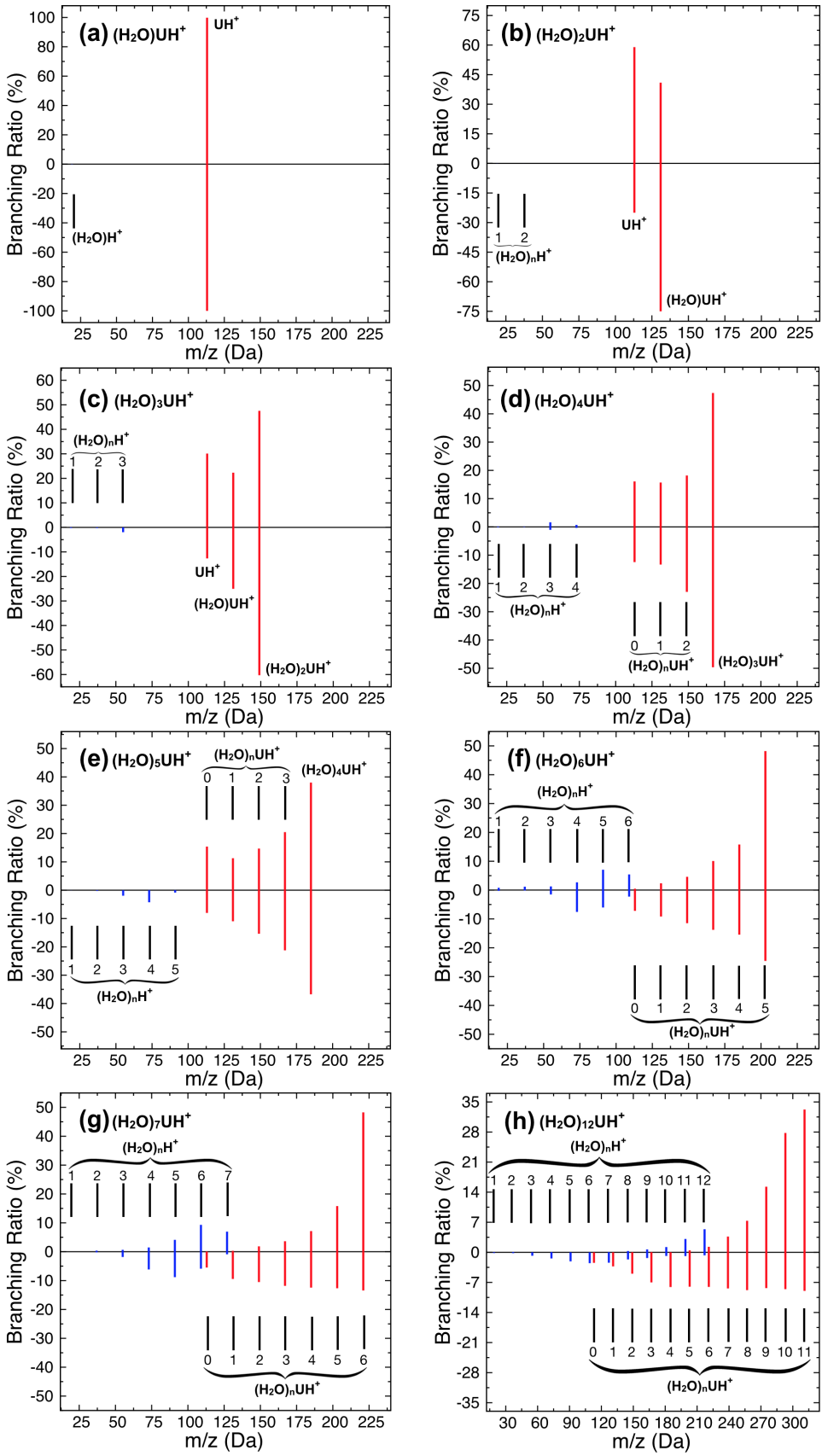

Fig. 10 Simulated mass spectra (positive area) of the charged fragments after 15 ps simulation time (fragments $(H_2O)_nH^+$ in red and $(H_2O)_nUH^+$ in blue) from isomers (a) 1a, (b) 2b, (c) 3b, (d) 4b, (e) 5d, (f) 6f, (g) 7d, and (h) 12c. The counterparts in experiment are plotted (negative area). Data for isomer 11d are presented in Figure S15 in the ESI. For $(H_2O)_{12}UH^+$, experimental values were obtained from collision with Ne. For comparison, all experimental data obtained from collision with Ne are presented in Figure S16 in the ESI.

Notes and references

1 R. N. Hayes and M. L. Gross, *Methods Enzymol.*, Elsevier, 1990, vol. 193, pp. 237–263.

2 R. A. Coates and P. Armentrout, *Phys. Chem. Chem. Phys.*, 2018, **20**, 802–818.

3 Y. Ma, Q. Li, H. Van den Heuvel and M. Claeys, *Rapid Commun. Mass Spectrom.*, 1997, **11**, 1357–1364.

4 S. M. Chowdhury, X. Du, N. Tolic, S. Wu, R. J. Moore, M. U. Mayer, R. D. Smith and J. N. Adkins, *Anal. Chem.*, 2009, **81**, 5524–5532.

5 C. C. Nelson and J. A. McCloskey, *J. Am. Soc. Mass Spectrom.*, 1994, **5**, 339–349.

6 E. R. Molina, D. Ortiz, J.-Y. Salpin and R. Spezia, *J. Mass Spectrom.*, 2015, **50**, 1340–1351.

7 D. R. Carl, R. M. Moision and P. B. Armentrout, *Int. J. Mass Spectrom.*, 2007, **265**, 308–325.

8 T. E. Hofstetter and P. B. Armentrout, *J. Phys. Chem. A*, 2013, **117**, 1110–1123.

9 R. A. Coates and P. Armentrout, *J. Phys. Chem. A*, 2017, **121**, 3629–3646.

10 S. Zamith, J.-M. L'Hermite, L. Dontot, L. Zheng, M. Rapacioli, F. Spiegelman and C. Joblin, *J. Chem. Phys.*, 2020, **153**, 054311.

11 P. D. Schnier, W. D. Price, R. A. Jockusch and E. R. Williams, *J. Am. Chem. Soc.*, 1996, **118**, 7178–7189.

12 R. Dunbar and T. McMahon, *Science*, 1998, **279**, 194–197.

13 S. E. Rodriguez-Cruz, R. A. Jockusch and E. R. Williams, *J. Am. Chem. Soc.*, 1998, **120**, 5842–5843.

14 F. O. Talbot, T. Tabarin, R. Antoine, M. Broyer and P. Dugourd, *J. Chem. Phys.*, 2005, **122**, 074310.

15 R. A. Zubarev, N. L. Kelleher and F. W. McLafferty, *J. Am. Chem. Soc.*, 1998, **120**, 3265–3266.

16 A. Ehlerding, C. S. Jensen, J. A. Wyer, A. I. Holm, P. Jørgensen, U. Kadhane, M. K. Larsen, S. Panja, J. C. Poully, E. S. Worm, H. Zettergren, P. Hvelplund and S. B. Nielsen, *Int. J. Mass Spectrom.*, 2009, **282**, 21–27.

17 K. McQuinn, F. Hof and J. S. McIndoe, *Int. J. Mass Spectrom.*, 2009, **279**, 32–36.

18 D. R. Carl and P. B. Armentrout, *ChemPhysChem*, 2013, **14**, 681–697.

19 S. T. Graul and R. R. Squires, *Int. J. Mass Spectrom. Ion Process*, 1989, **94**, 41–61.

20 S. Wei, W. Tzeng, R. Keesee and A. Castleman Jr, *J. Am. Chem. Soc.*, 1991, **113**, 1960–1969.

21 D. J. Goebbert, H. Chen and P. G. Wenthold, *J. Mass Spectrom.*, 2006, **41**, 242–247.

22 N. Haag, B. Liu, S. B. Nielsen, H. Zettergren, P. Hvelplund, B. Manil, B. A. Huber, H. A. B. Johansson, H. T. Schmidt and H. Cederquist, *Journal of Physics: Conference Series*, 2009, **194**, 012053.

23 B. Liu, S. B. Nielsen, P. Hvelplund, H. Zettergren, H. Cederquist, B. Manil and B. A. Huber, *Phys. Rev. Lett.*, 2006, **97**, 133401.

24 V. H. Nguyen, C. Afonso and J.-C. Tabet, *Int. J. Mass Spectrom.*, 2011, **301**, 224–233.

25 S. C. Shuck, K. L. Rose and L. J. Marnett, *Chem. Res. Toxicol.*, 2014, **27**, 136–146.

26 M. Castrovilli, P. Markush, P. Bolognesi, P. Rousseau, S. Maclot, A. Cartoni, R. Delaunay, A. Domaracka, J. Kočišek, B. Huber and L. Avaldi, *Phys. Chem. Chem. Phys.*, 2017, **19**, 19807–19814.

27 A. Bera, B. Concina, B. Schindler, G. P. Renois, G. Karras, I. Compagnon, A. Bhattacharya and F. Lépine, *Int. J. Mass Spectrom.*, 2018, **431**, 15–21.

28 S. J. Klippenstein, *J. Chem. Phys.*, 1992, **96**, 367–371.

29 T. Baer and W. L. Hase, *Unimolecular Reaction Dynamics: Theory and Experiments*, Oxford University Press on Demand, 1996, vol. 31.

30 N. Metropolis and S. Ulam, *J. Am. Stat. Assoc.*, 1949, **44**, 335–341.

31 A. F. Voter, *Radiation Effects in Solids*, Springer, 2007, pp. 1–23.

32 A. Shukla, R. Tosh, Y. Chen and J. Futrell, *Int. J. Mass Spectrom. and Ion Process*, 1995, **146**, 323–338.

33 E. Martínez-Núñez, A. Fernández-Ramos, S. A. Vázquez, J. M. Marques, M. Xue and W. L. Hase, *J. Chem. Phys.*, 2005, **123**, 154311.

34 H. Bednarski, K. Sohlberg, M. Domański, J. Weszka, G. Adamus, M. Kowalczuk and V. Cozan, *Int. J. Mass Spectrom.*, 2011, **304**, 15–24.

35 A. Martin Somer, V. Macaluso, G. L. Barnes, L. Yang, S. Pratihar, K. Song, W. L. Hase and R. Spezia, *J. Am. Soc. Mass Spectrom.*, 2020, **31**, 2–24.

36 W.-L. Yim and Z.-f. Liu, *J. Am. Chem. Soc.*, 2001, **123**, 2243–2250.

37 S. O. Meroueh, Y. Wang and W. L. Hase, *J. Phys. Chem. A*, 2002, **106**, 9983–9992.

38 J. Liu, K. Song, W. L. Hase and S. L. Anderson, *J. Chem. Phys.*, 2003, **119**, 3040–3050.

39 R. Spezia, J.-Y. Salpin, M.-P. Gaigeot, W. L. Hase and K. Song, *J. Phys. Chem. A*, 2009, **113**, 13853–13862.

40 R. Spezia, A. Cimas, M.-P. Gaigeot, J.-Y. Salpin, K. Song and W. L. Hase, *Phys. Chem. Chem. Phys.*, 2012, **14**, 11724–11736.

41 D. Ortiz, P. Martin-Gago, A. Riera, K. Song, J.-Y. Salpin and R. Spezia, *Int. J. Mass Spectrom.*, 2013, **335**, 33–44.

42 A. Martín-Sómer, M. Yáñez, M.-P. Gaigeot and R. Spezia, *J. Phys. Chem. A*, 2014, **118**, 10882–10893.

43 R. Spezia, J. Martens, J. Oomens and K. Song, *Int. J. Mass Spectrom.*, 2015, **388**, 40–52.

44 R. Spezia, S. B. Lee, A. Cho and K. Song, *Int. J. Mass Spectrom.*, 2015, **392**, 125–138.

45 I. V. Schweigert, *J. Phys. Chem. A*, 2015, **119**, 2747–2759.

46 E. R. Molina, A. Eizaguirre, V. Haldys, D. Urban, G. Doisneau, Y. Bourdreux, J.-M. Beau, J.-Y. Salpin and R. Spezia, *ChemPhysChem*, 2017, **18**, 2812–2823.

47 A. Malik, L. A. Angel, R. Spezia and W. L. Hase, *Phys. Chem. Chem. Phys.*, 2020, **22**, 14551–14559.

48 S. Li and E. R. Bernstein, *J. Chem. Phys.*, 1992, **97**, 792–803.

49 C. Bobbert, S. Schütte, C. Steinbach and U. Buck, *Eur. Phys. J. D*, 2002, **19**, 183–192.

50 J. M. Bakker, R. K. Sinha, T. Besson, M. Brugnara, P. Tosi, J.-Y. Salpin and P. Maître, *J. Phys. Chem. A*, 2008, **112**, 12393–12400.

51 P. Markush, P. Bolognesi, A. Cartoni, P. Rousseau, S. Maclot, R. Delaunay, A. Domaracka, J. Kocisek, M. C. Castrovilli, B. A. Huber and L. Avaldi, *Phys. Chem. Chem. Phys.*, 2016, **18**, 16721–16729.

52 P. Dawson, *Int. J. Mass Spectrom. Ion Process*, 1982, **43**, 195–209.

53 S. Zamith, P. Labastie and J.-M. L'Hermite, *J. Chem. Phys.*, 2012, **136**, 214301.

54 I. Braud, S. Zamith, J. Cuny, L. Zheng and J.-M. L'Hermite, *J. Chem. Phys.*, 2019, **150**, 014303.

55 M. Elstner and G. Seifert, *Philos. Trans. R. Soc. A-Math. Phys. Eng. Sci.*, 2014, **372**, 20120483.

56 M. Elstner, D. Porezag, G. Jungnickel, J. Elsner, M. Haugk, T. Frauenheim, S. Suhai and G. Seifert, *Phys. Rev. B*, 1998, **58**, 7260–7268.

57 D. Porezag, T. Frauenheim, T. Köhler, G. Seifert and R. Kaschner, *Phys. Rev. B*, 1995, **51**, 12947–12958.

58 G. Seifert, D. Porezag and T. Frauenheim, *Int. J. Quantum Chem.*, 1996, **58**, 185–192.

59 M. Rapacioli, F. Spiegelman, D. Talbi, T. Mineva, A. Goursot, T. Heine and G. Seifert, *J. Chem. Phys.*, 2009, **130**, 244304.

60 A. Simon, M. Rapacioli, J. Mascetti and F. Spiegelman, *Phys. Chem. Chem. Phys.*, 2012, **14**, 6771–6786.

61 A. Simon and F. Spiegelman, *Comput. Theor. Chem.*, 2013, **1021**, 54–61.

62 A. Simon, M. Rapacioli, E. Michoulier, L. Zheng, K. Korchagina and J. Cuny, *Mol. Simul.*, 2019, **45**, 249–268.

63 K. A. Korchagina, A. Simon, M. Rapacioli, F. Spiegelman and J. Cuny, *J. Phys. Chem. A*, 2016, **120**, 9089–9100.

64 K. A. Korchagina, F. Spiegelman and J. Cuny, *J. Phys. Chem. A*, 2017, **121**, 9485–9494.

65 K. Korchagina, A. Simon, M. Rapacioli, F. Spiegelman, J.-M. L'Hermite, I. Braud, S. Zamith and J. Cuny, *Phys. Chem. Chem. Phys.*, 2017, **19**, 27288–27298.

66 A. Simon, M. Rapacioli, G. Rouaut, G. Trinquier and F. Gadéa, *Philos. Trans. R. Soc. A*, 2017, **375**, 20160195.

67 M. Rapacioli, S. Cazaux, N. Foley, A. Simon, R. Hoekstra and T. Schlatholter, *Phys. Chem. Chem. Phys.*, 2018, **20**, 22427–22438.

68 J. Cuny, J. Cerda Calatayud, N. Ansari, A. A. Hassanali, M. Rapacioli and A. Simon, *J. Phys. Chem. B*, 0, **0**, null.

69 A. Warshel and M. Levitt, *J. Mol. Biol.*, 1976, **103**, 227–249.

70 C. Iftner, A. Simon, K. Korchagina, M. Rapacioli and F. Spiegelman, *J. Chem. Phys.*, 2014, **140**, 034301.

71 E. Kukk, D. Ha, Y. Wang, D. G. Piekarski, S. Diaz-Tendero, K. Kooser, E. Itälä, H. Levola, M. Alcamí, E. Rachlew and F. Martín, *Phys. Rev. A*, 2015, **91**, 043417.

72 T. Heine, M. Rapacioli, S. Patchkovskii, J. Frenzel, A. Köster, P. Calaminici, H. Duarte, S. Escalante, R. Flores-Moreno and A. Goursot, *deMonNano, http://demon-nano.ups-tlse.fr/*, 2009.

73 Y. Sugita and Y. Okamoto, *Chem. Phys. Lett.*, 1999, **314**, 141–151.

74 D. J. Earl and M. W. Deem, *Phys. Chem. Chem. Phys.*, 2005, **7**, 3910–3916.

75 S. Nosé, *J. Chem. Phys.*, 1984, **81**, 511–519.

76 W. G. Hoover, *Phys. Rev. A*, 1985, **31**, 1695–1697.

77 S. Ø. Pedersen, C. S. Byskov, F. Turecek and S. B. Nielsen, *J. Phys. Chem. A*, 2014, **118**, 4256–4265.

78 F. Weigend and R. Ahlrichs, *Phys. Chem. Chem. Phys.*, 2005, **7**, 3297–3305.

79 F. Weigend, *Phys. Chem. Chem. Phys.*, 2006, **8**, 1057–1065.

80 M. J. Frisch, G. W. Trucks, H. B. Schlegel, G. E. Scuseria, M. A. Robb, J. R. Cheeseman, G. Scalmani, V. Barone, B. Mennucci, G. A. Petersson and *et. al.*, Gaussian 03 Revision A.1. Gaussian Inc.: Pittsburgh PA., 2003.

81 G. Bussi, D. Donadio and M. Parrinello, *J. Chem. Phys.*, 2007, **126**, 014101.